Design of Multi-Phase Combined Windings for Bearingless Machines

Anvar Khamitov* *Student Member, IEEE*, Eric L. Severson* *Senior Member, IEEE**Department of Electrical and Computer Engineering, University of Wisconsin-Madison, Madison, WI 53706 USA

Abstract—A generalized multi-phase (MP) combined winding design procedure for bearingless machines is proposed and developed. Using this procedure, new bearingless motor windings can be designed and conventional motor designs with MP windings can be transformed into bearingless motors by simply modifying the phase currents. The resulting MP winding is excited by two current components - one responsible for torque creation and another for suspension force creation. By applying the appropriate Clarke transformation, independent control of force and torque can be achieved. Although there are numerous papers in the literature studying bearingless machines with MP windings and their advantages, this is the first paper to provide a formal design procedure that can be applied to any MP winding configuration. The proposed approach can be used to realize popular winding designs, including concentrated- and fractional-slot windings, and is applicable to all radial-flux bearingless machines. The paper uses the Maxwell stress tensor to formulate the force/torque model for the MP combined winding and uses the results to derive design requirements. A sequence of winding design steps is proposed and used to design example MP combined windings. Experimental validation is provided using a six-phase bearingless induction machine prototype.

Index Terms—Bearingless drive, bearingless motor, generalized Clarke transformation, multi-phase winding, self-bearing motor

NOMENCLATURE

	Nomenclature
α	Angle along the inner bore of the stator.
$\alpha_{ m peak}$	Angular location of airgap magnetic field peak.
$\alpha_{\mathrm{ph},s}, \alpha_{\mathrm{ph},t}$	Spacing between phases in susp. and torque
	star of slots.
$\alpha_{\mathrm{ph,w}}$	Mech. angle between adj. phases, see Fig. 2b.
α_s , α_t	Susp. and torque cur. phase separation angles.
α_u	Angle between adjacent slots, $=\frac{2\pi}{Q}$.
$\alpha_{\mathrm{w0},h}$	Phase shift angle at harmonic h .
$\alpha_{\mathrm{w},k}$	Angluar location of magnetic field harmonic \boldsymbol{h}
	due to phase $k_1 = \alpha_{w0,h}/h + (k-1)\alpha_{ph,w}$.
α_z	Angle between adjacent phasors in star of
	slots, $=\frac{2\pi}{Q}t$.
$\delta_{ m eff}$	Effective airgap length.
θ, θ_m	Electrical and mechanical rotor angle.
$\sigma_{\rm n}, \sigma_{\rm tan}$	Normal and tangential components of stress
	acting on the surface of the rotor.
ϕ	Force vector angle.
ϕ_s, ϕ_t	Susp. and torque current phase angles.
$A'_{c,ph,h}$	Peak of per ampere circumferential current
	density at harmonic $h_1 = \frac{2}{\pi} z_Q z_c \hat{k}_{w,h}$.
$A_k(\alpha)$	Linear current density at phase k .
$B_{\delta}, \hat{B}_{\delta}$	Magnetizing field and its amplitude at a space

This work was supported in part by the USA National Science Foundation under Grant #1942099.

harmonic h.

$B_{ m n/tan}$	Normal and tangential components of the air-
	gap magnetic field.
$B_{\rm n,r}, B_{\rm n,s}$	Normal magnetic field due to rotor and stator.
$B_{n/tan,w,k}$	Normal or tangential component of the airgap
, ,	magnetic field due to winding phase k .
$oldsymbol{F}$	Array of radial force components and torque,
	$= [F_x \ F_y \ \tau]^T.$
f	Current excitation frequency.
h	Spatial harmonic order.
h_1, h_2	Harmonics that contribute to the force creation:
	$h_1 = p - 1, \ h_2 = p + 1.$
$m{i}$	Array of phase currents, = $[i_1 \ i_2 \ i_k \ i_m]^T$.
I_s, I_t	Suspension and torque current amplitudes.
I_x, I_y	Current components that create F_x and F_y .
i_s,i_t	Array of suspension and torque phase currents.
$i_{s,k}, i_{t,k}$	Suspension and torque current at phase k .
k	Phase order, $=1, 2,, m$.
$\hat{k}_{d,h},\hat{k}_{p,h}$	Distribution and pitch factors at harmonic h .
k_f, k_t	Total force or torque per ampere.
$\hat{k}_{w,h}$	Winding factor at harmonic h , = $\hat{k}_{d,h}\hat{k}_{p,h}$.
L, V_r	Axial length, rotor volume.
m	Number of drive connections.
m_s, m_t	Susp. and torque effective number of phases.
\mathbb{N}	Set of natural numbers.
p, p_s	Torque and suspension pole-pairs.
Q	Number of slots.
r	Airgap radius.
t	Greatest common divisor (gcd) of Q and h .
$T_{m{m}}$	Matrix, mapping from phase currents i to
	forces/torque F . Rows are $[T_{mx} T_{my} T_{mt}]^T$.
T_{md}	Force row matrix, $= T_{mx}$ or T_{my} .
$T_{md,k}$	Force per ampere per phase, element of T_{md} .
T_{mt}	Torque row matrix.
$\hat{T}_{mf,h_{1/2}}$	Peak force per ampere per phase due to har-
V , 1/2	monic h_1 or h_2 .
$T_{mt,k}$	Torque per ampere per phase, element of T_{mt} .
\hat{T}_{mt}	Peak torque per ampere per phase.
y	Coil span in number of slots.
z_c, z_Q	Number of coils per phase, number of series
~	

I. Introduction

turns per coil.

Magnetic levitation technologies have potential to replace conventional motor bearings and provide contact-free and lubricant-free support of the motor shaft. This eliminates any point of wear, bearing friction, and contamination issues. Traditionally, magnetic bearings have been used to implement magnetic levitation. However, over the past decades, bearingless motors have been developed that can simultaneously

2

operate as a motor and magnetic bearing [1], thus, having the potential to reduce the system complexity. The radial x and y forces are typically created by a radial bearingless motor to stabilize the 2 degrees of freedom (DOF), while the other 3 DOF (tilting around x and y and displacement along z) are stabilized by another bearingless motor, magnetic bearing, or passively as in bearingless slice motors [2].

First generation bearingless machines used two separate windings to produce suspension forces and torque. In these machines, the suspension winding typically occupies an order of magnitude more slot space than is required during nominal operation in order to meet a worst-case force requirement. This leads to machine designs with decreased power density, increased ohmic and iron losses, and leakage inductance [3]. To solve these problems, several combined winding configurations have been developed, where each phase winding is responsible for both force and torque creation. Four distinct combined winding categories are found in the literature: "multiphase (MP)" [4]-[7], "dual-purpose no-voltage (DPNV)" [8]-[10], "multi-sector" [11], and "middle-point current injection" [12] windings. Of these winding types, MP and DPNV are most promising for high performance control as independent motor (torque and field weakening) and suspension (x and y forces) operation can be achieved through space vector transformations (Generalized Clarke transformation).

While the MP winding is inherently compatible with more stator designs than the DPNV winding, there is currently no generalized method that can be applied to design an MP combined winding. Study [13] provides a list of MP winding configurations and determines whether force and torque decoupling is possible. However, the results are limited to concentrated windings with one coil per phase, and no analytic design procedure was provided to design an MP winding for an arbitrary number of slots, poles, and phases. This paper fills this gap by analytically deriving a set of design requirements and proposing a formal winding design procedure, which pertain to all radial-flux bearingless machines. In these machines, torque and radial suspension suspension forces are created from the interaction between radial magnetic fields. The derivations in this paper are provided for nonsalient machines, using surface permanent magnet (SPM) and induction machines as examples. This work is analogous to [14], which derived design requirements and proposed a generalized design procedure for DPNV windings.

The core contributions of this paper are:

- Determination of which combinations of electric machine slots, poles, and phases can be used to design symmetric MP combined windings (Section V).
- Identification of design criteria that allow an MP combined winding to be operated from a DPNV drive (Section VI).
- Proposal of a generalized MP combined winding design theory based on the star of slots approach and the results from Sections III and V (Section VII).

Section II introduces MP combined windings and reviews relevant literature. Section III develops a force/torque model using the Maxwell stress tensor and Section IV develops winding analysis concepts for the MP combined winding by extending standard fractional slot winding theory [15]. Using the results from these sections, Section V develops design requirements in the form of constraint equations and Section VI makes a comparison to the DPNV winding. These design requirement can also be used to determine whether existing MP motor designs can be transformed into bearingless machines through control action alone. Section VII proposes an MP combined winding design procedure for symmetric windings using the star of slots approach. Section VIII validates the developed theory using finite element analysis (FEA) and hardware measurements from a six-phase bearingless induction machine prototype. A conference version of this paper was previously published in [16] which did not include the experimental validation provided in this paper.

II. MP COMBINED WINDINGS

It is well-known that MP machines are able to produce multiple magnetic field harmonics in the airgap [17]. Bearingless motors with MP combined windings use this capability to create one field for torque and a second field for suspension. These windings have m>3 distinct connections to the bearingless drive, as shown in Fig. 1. Depending on the drive design requirement, the phases can share a single neutral point or be grouped to have several neutral points.

The phase currents in conventional MP machines can be transformed into multiple independent space vectors located in independent rotating reference frames (orthogonal subspaces) [18]. Study [19] presented a Generalized Clarke transformation matrix for symmetrical MP windings that is used to obtain these independent space vectors. In conventional MP machines, a single rotating reference frame represents the torque creation, while other reference frames represent the machine's harmonic patterns which highlight the possible unbalance among the phases [17]. A number of other studies have been presented that use these reference frames for different nontraditional purposes. Study [20], for example, presented decoupled dq axes control in multi-three-phase induction machines. Study [21] surveyed innovative ways of exploiting additional DOFs of MP systems. One such example is series connected MP motors which are connected to a single inverter and the torque in each motor is created independently (represented by two independent space vectors).

The bearingless machine requires p pole-pairs on the rotor and stator winding to create torque, and $p_s = p \pm 1$ polepairs on the stator winding to create suspension forces. This implies that the MP combined winding must be intentionally designed to be capable of creating magnetic field harmonics at p and p_s . As a result, the same theory that is used in MP machines can be extended to MP combined windings to independently control radial suspension forces and torque in two independent rotating frames. However, the following two requirements must be met to ensure that the winding is:

- 1) symmetric; that is, a rotating magnetic field is created when supplied from a symmetrical supply.
- 2) capable of independently controlling force and torque.

The winding layout and the current excitation must be studied and used to derive these requirements in terms of

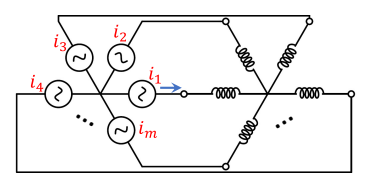


Fig. 1. Circuit diagram with m drive connections.

the machine parameters (number of phases m, torque p and suspension p_s pole-pairs, and slots Q). For this, the bearing-less machine force/torque matrix model is presented in the following section and used in later sections.

III. MP COMBINED WINDING MATRIX MODEL

This section presents a bearingless machine matrix model and develops analytic expressions for the created forces and torque in terms of the phase currents and the rotor angle.

A. Force/Torque Matrix Model

The operating theory for a bearingless machine can be represented using matrices as presented in [2] and [22]. This model shows the relationship between the created forces/torque, the drive terminal currents, and the rotor position. For a centered rotor position, this relationship can be expressed as

$$F(\theta_m) = T_m(\theta_m)i \tag{1}$$

where T_m is a matrix used to map the phase currents i into the forces and torque they produce on the rotor. For a machine with m phases, T_m is of the form:

$$\boldsymbol{T_m} = \begin{bmatrix} \boldsymbol{T_{mx}} \\ \boldsymbol{T_{my}} \\ \boldsymbol{T_{mt}} \end{bmatrix} = \begin{bmatrix} T_{mx,1} & T_{mx,2} & \dots & T_{mx,m} \\ T_{my,1} & T_{my,2} & \dots & T_{my,m} \\ T_{mt,1} & T_{mt,2} & \dots & T_{mt,m} \end{bmatrix}$$
(2)

Having the phase currents $i = [i_1 \ i_2 \ ... \ i_m]^T$ and using (2), the model (1) can be rewritten for each force and torque as

$$F_d(\theta) = \mathbf{T_{md}} \mathbf{i} = \sum_{k=1}^m F_{d,k}(\theta) = \sum_{k=1}^m T_{md,k}(\theta) i_k \qquad (3)$$

$$\tau(\theta) = \mathbf{T_{mt}} \mathbf{i} = \sum_{k=1}^{m} \tau_k(\theta) = \sum_{k=1}^{m} T_{mt,k}(\theta) i_k$$
 (4)

where d=x or y. $F_{d,k}$ and τ_k are the force and torque created by a phase winding k. Each T_m matrix entry can be interpreted as a per ampere force or torque created when only a single phase is excited.

Suppose that the phase currents can be written as the sum of two current arrays for suspension i_s and for torque i_t :

$$\boldsymbol{i} = \begin{bmatrix} i_1 \\ i_2 \\ \dots \\ i_m \end{bmatrix} = \boldsymbol{i_s} + \boldsymbol{i_t} = \begin{bmatrix} i_{s,1} \\ i_{s,2} \\ \dots \\ i_{s,m} \end{bmatrix} + \begin{bmatrix} i_{t,1} \\ i_{t,2} \\ \dots \\ i_{t,m} \end{bmatrix}$$
(5)

Substituting (5) into (3)-(4), the design requirements requirements presented in Section II can be rewritten as: 1) symmetry: $T_{md}i_s$ and $T_{mt}i_t$ are independent of the rotor angle θ , and 2) independent force and torque creation: $T_{md}i_t=0$ and $T_{mt}i_s=0$. Depending on the T_m matrix, the desired i_s and i_t satisfying these constraints can be determined and the MP combined winding design requirements can be derived. The derivation of the entries of T_m is now presented.

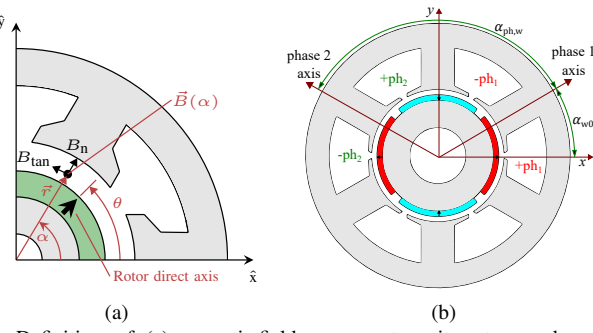


Fig. 2. Definitions of: (a) magnetic field components, unit vectors, and angles $(\alpha \text{ and } \theta)$ and (b) axes and winding phase angles $(\alpha_{\text{ph,w}} \text{ and } \alpha_{\text{w0}})$; $+p_1$ and $-p_1$ denote phase 1 coil sides going into and out of the page, respectively.

B. Derivation of T_m matrix entries

The Maxwell stress tensor is used to calculate force/torque:

$$\vec{\sigma} = \begin{bmatrix} \sigma_{\rm n} \\ \sigma_{\rm tan} \end{bmatrix} = \begin{bmatrix} \frac{1}{2\mu_0} (B_{\rm n}^2 - B_{\rm tan}^2) \\ \frac{1}{\mu_0} B_{\rm n} B_{\rm tan} \end{bmatrix} \tag{6}$$

where σ_n and σ_{tan} are the normal and tangential components of the per unit area force (stress) acting on the surface of the rotor. This force is created from the interaction between the tangential (B_{tan}) and normal (B_n) components of the magnetic field in the airgap, which are depicted in Fig. 2a. These stresses can be integrated over the rotor's airgap surface S to determine the net forces and torque acting on the rotor:

$$F_x = \int_S \vec{\sigma} \cdot \hat{\mathbf{x}} \, \mathrm{d}S, \ F_y = \int_S \vec{\sigma} \cdot \hat{\mathbf{y}} \, \mathrm{d}S, \ \tau = \int_S \vec{r} \times \vec{\sigma} \, \mathrm{d}S \quad (7)$$

where \vec{r} is the airgap radius vector (see Fig. 2a), and \hat{x} and \hat{y} are the unit vectors.

The T_m matrix entries are now determined using the following steps. When phase k is excited by current i_k ,

- 1) expressions for the airgap magnetic field normal $B_{n,k}$ and tangential $B_{tan,k}$ components are determined;
- 2) $F_{x,k}$, $F_{y,k}$, τ_k are determined using (7); and
- 3) finally, the T_m matrix entries are calculated from $T_{mx,k} = F_{x,k}/i_k$, $T_{my,k} = F_{y,k}/i_k$, and $T_{mt,k} = \tau_k/i_k$.

As will be shown, each T_m matrix entry is a function of the fixed machine parameters and the rotor angle, but not the phase currents. The above steps are now illustrated.

1) Step 1: The total magnetic field in the airgap is created by rotor and stator magnetic field sources (shown for B_n):

$$B_{\rm n} = B_{\rm n,r} + B_{\rm n,s} \tag{8}$$

In SPM machines, $B_{\rm n,s}=B_{\rm n,w}$ is created by stator winding currents and $B_{\rm n,r}$ is created by permanent magnets described by $B_{\rm n,r}=B_{\delta}=\hat{B}_{\delta}\cos\left(p\alpha-\theta\right)$ (also known as the magnetizing field). Stator winding currents must create both p and p_s pole-pair fields to interact with the rotor's p pole-pair field and create torque and forces.

In induction machines, $B_{\rm n,s}=B_{\rm n,w}$ is also created by stator winding currents and $B_{\rm n,r}$ is created by currents induced in the rotor windings/bars. The stator winding currents create the magnetizing field B_{δ} and the reaction field to the rotor field $B'_{\rm n,r}=-B_{\rm n,r}$ at p pole-pairs, and suspension field at p_s polepairs. When a pole-specific rotor structure is used, the stator

 p_s pole-pair field does not induce currents in the rotor and no reaction field is created, see [23].

The total magnetic field from stator windings $B_{n,w}$ can be expressed as the sum of fields from each phase winding. The field from each phase winding is determined using the well-known linear current density $A_k(\alpha)$ that can be expressed as the sum of all space harmonics (shows the current distribution along the inner bore of the stator),

$$A_k(\alpha) = \frac{i_k}{r} \sum_{h=1}^{\infty} A'_{c, \text{ph}, h} \sin\left(h[\alpha - \alpha_{\text{w}, k}]\right)$$
 (9)

where $A'_{c,\mathrm{ph},h}$ is a normalized parameter showing the effective number of turns per radian for the space harmonic h and $\alpha_{\mathrm{w},k}$ is the angular location where the current density at harmonic h is zero. For torque and suspension pole-pairs, $A'_{c,\mathrm{ph},h}$ is denoted as $A'_{c,\mathrm{ph},t}$ and $A'_{c,\mathrm{ph},s}$.

Using (9), the winding magnetic field components created by a phase k can be determined as

$$B_{\text{n,w},k} = \frac{\mu_0 i_k}{\delta_{\text{eff}}} \sum_{h=1}^{\infty} \frac{A'_{c,\text{ph},h}}{h} \cos\left(h[\alpha - \alpha_{\text{w},k}]\right)$$
(10)

$$B_{\text{tan,w},k} = -\frac{\mu_0 i_k}{r} \sum_{h=1}^{\infty} A'_{c,\text{ph},h} \sin\left(h[\alpha - \alpha_{\text{w},k}]\right)$$
(11)

These expressions are used to derive per phase forces and torque in the following steps.

2) Steps 2 and 3: The forces and torque $F_{x,k}$, $F_{y,k}$, τ_k created by phase k current are determined using (7). The torque per phase τ_k is calculated by substituting (6) into (7):

$$\tau_k = \frac{r^2 L}{\mu_0} \int_0^{2\pi} B_{\mathrm{n},k} B_{\mathrm{tan},k} \,\mathrm{d}\alpha \tag{12}$$

Evaluating (12) for harmonic p and dividing the result by i_k , entries of the row T_{mt} are obtained:

$$T_{mt,k} = -\hat{T}_{mt}\sin\left(\theta - p\alpha_{w,k}\right), \ \hat{T}_{mt} = \frac{V_r \hat{B}_{\delta} A'_{c,ph,t}}{r} \quad (13)$$

which shows created torque per ampere due to phase k.

The T_{mx} and T_{my} entries can be derived similarly. The difference from torque creation is that the force is created from the interaction between adjacent harmonics h and $h\pm 1$. At h=p, it can be shown that the T_{mx} and T_{my} entries are:

$$T_{md,k} = \hat{T}_{mf,h_1} f_d(\theta - h_1 \alpha_{w,k}) \pm \hat{T}_{mf,h_2} f_d(\theta - h_2 \alpha_{w,k})$$
(14)

which shows created force per ampere due to phase k. Here, the \pm term is + for d=x and - for d=y; f_x and f_y are cosine and sine functions. \hat{T}_{mf,h_1} and \hat{T}_{mf,h_2} are (15), where $h_s=h_1$ or h_2 .

$$\hat{T}_{mf} = \frac{V_r \hat{B}_\delta A'_{c, \text{ph}, h_s}}{2r} \left(\frac{1}{h_s \delta} + \frac{h_s - p}{r} \right) \tag{15}$$

Section V will use the results (13)-(14) and (3)-(4) to derive conditions for viable windings.

IV. MP COMBINED WINDING ANALYSIS

The standard fractional slot winding analysis techniques presented in textbooks such as [15] are now extended to enable analysis of MP combined windings for bearingless motors. The results of this analysis will be used to derive winding requirements in Section V and to develop the winding design procedure proposed in Section VII.

A. Star of Slots

It is common practice to design conventional stator windings (non-bearingless) using the "star of slots" diagram [15]. This diagram shows the phasor of a particular harmonic of back-EMF induced in each coil side. Using this diagram, the winding layout of the motor (phase assignment of the coil sides) can be determined. This approach can be analogously extended to MP combined windings, the key difference being that two winding harmonics are now considered, h=p (torque) and $h=p_s$ (force creation). This paper uses the terms "torque star of slots" and "suspension star of slots" to indicate that the star of slots diagram is drawn at harmonic p or p_s .

Example torque and suspension star of slots diagrams are shown in Fig. 3 for a motor with Q=8 slots, p=2, and $p_s=3$. The phasor of the first slot is drawn horizontally and subsequent phasors lag by $p\alpha_u$ (or $p_s\alpha_u$). Depending on the values of p and p_s , Fig. 3 shows that several slots can have the same phasor location. Further, the angle between the phasors of adjacent slots may not be equal to the angle between adjacent phasors. For example, Fig. 3b shows that the angle between slots 1 and 2 is 135° , while the angle between adjacent phasors (slots 1 and 4) is 45° . This phasor angle can be determined using the following equation [15]:

$$\alpha_z = \frac{2\pi}{O}t\tag{16}$$

where t is either gcd(Q, p) or $gcd(Q, p_s)$.

The winding design procedure proposed in Section VII leverages the star of slots diagram because it provides a convenient method to determine the winding's ability to create both p and p_s pole-pair fields in the airgap. The torque and suspension star of slots are used along with phasor summation properties to determine the effects of different phase-slot assignments on these harmonics, identify phase zones, and determine phase separation of current components to create the p and p_s pole-pair fields. While these aspects could be determined using winding function theory, this would require additional tools such as the Fourier Transform.

B. Winding Factor

The winding factor is useful for comparing windings. For double-layer windings, at harmonic h, it is defined as:

$$\hat{k}_{w,h} = \hat{k}_{d,h} \hat{k}_{p,h} \tag{17}$$

where $\hat{k}_{d,h}$ is a distribution factor that is found by summing all phasors assigned to one phase in the star of slots and $\hat{k}_{d,h}$ is a pitch factor that is determined by a coil span y:

$$\hat{k}_{d,h} = \left| \frac{1}{z_c} \sum_{i=1}^{z_c} e^{-j\alpha_{i,h}^e} \right|, \ \hat{k}_{p,h} = \sin\left(\frac{hy\alpha_u}{2}\right)$$
 (18)

Here, $\alpha_{i,h}^e$ is the phasor angle in the star of slots at harmonic h. It is desired to maximize $\hat{k}_{w,h} = \hat{k}_{d,h}\hat{k}_{p,h}$ (maximum is 1) for all magnetic field harmonics h that the designer wants to create in the airgap. These metrics are used in Section VII.

C. Effective number of phases

This subsection introduces the notion of an "effective" number of torque and suspension phases in the MP combined winding, which will prove useful later for deriving symmetry requirements. In conventional MP windings, the angle $\alpha_{\rm ph,w}$ (see Fig. 2) is translated to $p\alpha_{\rm ph,w}$ in the star of slots and $\alpha_{\rm ph,w}$ is selected to ensure that $p\alpha_{\rm ph,w}$ can be reduced to $2\pi/m$. In MP combined windings, the angle $\alpha_{\rm ph,w}$ corresponds to the angles α_t , α_s in the torque, suspension star of slots. These angles are not necessarily $2\pi/m$ and can be expressed as

$$\alpha_t = k_1 \frac{2\pi}{m}, \ \alpha_s = k_2 \frac{2\pi}{m} \tag{19}$$

where k_1 and k_2 are integer numbers. In mechanical radians, it must be true that $\alpha_{\rm ph,w}=\alpha_t/p=\alpha_s/p_s$. Substituting (19) into this expression, it can be shown that $k_1/k_2=p/p_s$. Since, p and p_s are co-prime, it must be true that $k_1=cp$ and $k_2=cp_s$, where c is an integer number. Picking the smallest positive values of $k_1=p$ and $k_2=p_s$, the phase separation angles for MP combined windings become:

$$\alpha_{\text{ph,w}} = \frac{2\pi}{m}, \ \alpha_t = p\frac{2\pi}{m}, \ \alpha_s = p_s\frac{2\pi}{m}$$
 (20)

This shows that $\alpha_{\rm ph,w}$ in MP combined windings must be constrained to $2\pi/m$. From this result, the following two observations can be drawn about MP combined windings:

- 1) The phases adjacent in the stator winding may not be adjacent in torque or suspension star of slots: e.g., with p=3 and m=4, $\alpha_t=\frac{3\pi}{2}$ and the torque phases in the star of slots have angles in the order of $0,\,\frac{3\pi}{2},\,\pi,\,\frac{\pi}{2}$ instead of $0,\,\frac{\pi}{2},\,\pi,\,\frac{3\pi}{2}$.
- 2) The effective number of phases for torque or suspension creation can be less than m: e.g., when m=8, p=6, and $p_s=7$, $\alpha_t=3\cdot\frac{360^\circ}{4}$ and $\alpha_s=7\cdot\frac{360^\circ}{8}$. These angles show 4 effective torque and 8 effective suspension phases.

Generally, for any MP combined winding, the number of effective torque and suspension phases can be calculated by reducing p/m or p_s/m until the numerator and the denominator are co-prime. The resulting denominator is the effective

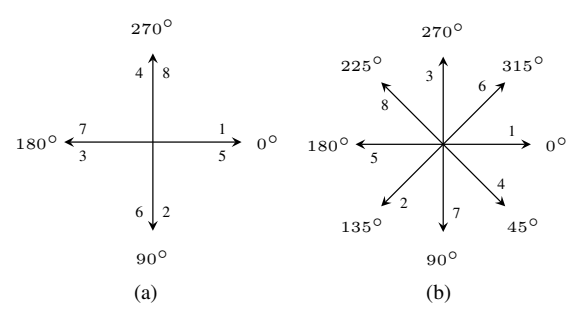


Fig. 3. Demonstration of star of slots diagrams for $Q=8,\ p=2,$ and $p_s=3$: (a) torque star of slots and (b) suspension star of slots.

number of phases. This can be directly calculated as (21), with the subscripts t and s indicating torque and suspension.

$$m_t = \frac{m}{\gcd(m, p)}, \ m_s = \frac{m}{\gcd(m, p_s)}$$
 (21)

The m_t and m_s phase numbers determine the spacing between phases in the torque and suspension star of slots:

$$\alpha_{\text{ph},t} = \frac{2\pi}{m_t}, \ \alpha_{\text{ph},s} = \frac{2\pi}{m_s} \tag{22}$$

The distinction between α_t and $\alpha_{\mathrm{ph},t}$ (or α_s and $\alpha_{\mathrm{ph},s}$) is similar to the discussion in Section IV-B, where the phasor angle α_z is analogous to $\alpha_{\mathrm{ph},t}$ (or $\alpha_{\mathrm{ph},s}$), while the slot angles in star of slots $p\alpha_u$ and $p_s\alpha_u$ are analogous to α_t and α_s . Note that these angles are also apparent in the phase currents, which will have a phase spacing of $\alpha_{\mathrm{ph},t}$ for torque i_t and $\alpha_{\mathrm{ph},s}$ for suspension i_s . However, the order that phase currents appear in an array is based on α_t for torque and α_s for suspension.

If the number of drive connections is even, the system is called "non-reduced" (non-loaded star configuration) [15, Ch 2.9.1]. In conventional winding design, the star of slots has pairs of phasors 180° apart, the phase system can be "reduced" by decreasing the original number of phases by half. If the new number of phases (after reduction) is even, a neutral point needs to be loaded. In MP combined windings, reducing the system is not possible because two phases that are 180° apart in the torque star of slots are $180^{\circ}p_s/p \neq 180^{\circ}$ apart in the suspension star of slots. Therefore, m in these derivations denotes the number of the drive connections of a non-reduced system rather than the number of torque or suspension phases.

V. MP COMBINED WINDING DESIGN REQUIREMENTS

MP combined windings must satisfy symmetry and independent force/torque creation requirements. This section determines which combinations of electric machine slots Q, pole-pairs p and p_s , and phases m can be used to design an MP machine that meets these requirements. This is a primary contribution of this paper. The design requirements are derived as constraint equations in Sections V-A and V-B and summarized in Table I.

A. Symmetry Requirements

Symmetry requirements ensure that a rotating magnetic field is created when the winding is fed from a symmetrical supply. The MP combined winding must meet the two standard requirements (typically considered for conventional machines [15]) and new requirements, all of which are now presented.

1) Review of standard requirements: The first requirement is that the number of coils per phase (z_c/m) must be an integer [15]. This is listed in Table I, where z_c is found as

$$z_c = \begin{cases} Q/2, & \text{single-layer winding} \\ Q, & \text{double-layer winding} \end{cases}$$
 (23)

The second requirement ensures that the phase spacing $\alpha_{\rm ph}=2\pi/m$ in the torque star of slots is an integer multiple

of the phasor angle α_z in (16). In an MP combined winding, this is analogously extended for both torque and suspension:

$$\frac{\alpha_{\text{ph},t}}{\alpha_z} \in \mathbb{N}, \ \frac{\alpha_{\text{ph},s}}{\alpha_{zs}} \in \mathbb{N}$$
 (24)

where α_{zs} is analogous to α_z , but calculated with $h = p_s$. Substituting (16) and (22), the requirements are rewritten as

$$\frac{Q}{m}\frac{\gcd(m,p)}{\gcd(Q,p)} \in \mathbb{N}, \ \frac{Q}{m}\frac{\gcd(m,p_s)}{\gcd(Q,p_s)} \in \mathbb{N}$$
 (25)

Since $Q/m \in \mathbb{N}$, it is also true that $\gcd(Q,p)/\gcd(m,p) \in \mathbb{N}$: $\gcd(Q,p) = b\gcd(m,p)$, where $b \in \mathbb{N}$. It can be shown that Q/m is a multiple of b. Therefore (25), and hence the second requirement in (24), is guaranteed to be satisfied for combined MP windings that meet the first symmetry requirement.

2) New requirements: Because the effective number of torque and suspension phases are not necessarily equal to m, additional symmetry requirements are needed to ensure that the MP combined winding can create rotating (not oscillating) p and p_s pole-pair fields. This can be articulated as that α_t and α_s cannot be multiples of π (or, equivalently: $m_t > 2$ and $m_s > 2$). Based on (20), these requirements are satisfied when p and p_s are not a multiple of m/2. This can be rewritten as:

$$\frac{2p}{m} \notin \mathbb{N}, \ \frac{2p_s}{m} \notin \mathbb{N} \tag{26}$$

3) Permissible Non-Symmetric Windings: Satisfying the conditions for a fully symmetric winding (summarized in the first two rows of Table I) requires $m \geq 5$ connections to the motor drive. However, example combined winding designs can be found in literature with m=3 and 4 phase connections, i.e. [2], [24], [25]. This section develops theory explaining these windings, showing that they can be achieved by relaxing (26) to allow $\frac{2p}{m} \in \mathbb{N}$. It is found that doing this can result in a viable bearingless machine, albeit with lower performance analogous to a single phase motor, with the machine having an oscillating (rather than rotating) magnetic field of p pole-pairs.

The analysis is presented through torque and force calculations. Torque is calculated by substituting (13) into (4). Each torque phase current must be in phase with $T_{mt,k}$ to create the maximum torque per ampere:

$$i_{t,k} = I_t \cos\left(\theta + \pi/2 - p\alpha_{w,k}\right) \tag{27}$$

Using complex numbers (phasors), (4) can be written as:

$$\tau = \frac{\hat{T}_{mt}I_t}{2} \Re \left\{ \sum_{k=1}^m e^{j2\left(\theta + \frac{\pi}{2} - p\alpha_{w0} - [k-1]\alpha_t\right)} + m \right\}$$
 (28)

If the symmetry requirements in Table I are satisfied, the torque is independent of rotor angle and (28) simplifies to

$$\tau = k_t I_t, \ k_t = m\hat{T}_{mt}/2 \tag{29}$$

where k_t is a torque per ampere constant. For windings that violate $\frac{2p}{m} \notin \mathbb{N}$ of (26), an oscillating field of p pole-pairs is created and the torque expression in (28) simplifies to

$$\tau = 2k_t I_t \sin^2\left(\theta - p\alpha_{w0}\right) \tag{30}$$

where the torque has so-called "single-phase characteristics". These windings have very high torque ripple because they are unable to create torque at certain rotor angular positions $(\theta = p\alpha_{w0})$, but do have a non-zero average torque (k_tI_t) over one rotor revolution.

To study the impact on force creation, force expressions are similarly determined. Each force phase current must be in phase with the $T_{md,k}$ term of (14):

$$i_{x,k} = I_x \cos(\theta - p_s \alpha_{w,k}), i_{y,k} = \pm I_y \sin(\theta - p_s \alpha_{w,k})$$

$$i_{s,k} = i_{x,k} + i_{y,k} = I_s \cos(\theta - p_s \alpha_{w,k} \mp \phi)$$
 (31)

where $I_s = \sqrt{I_x^2 + I_y^2}$, $\phi = \tan^{-1}\left(I_y/I_x\right)$ is the force angle, upper signs are for $p_s = h_1$ and lower signs are for $p_s = h_2$. The net force F_x is found in an analogous manner to (28):

$$F_x = \frac{I_x}{2} \left(\hat{T}_{mf,h1} \Re\{F_1 + F_2\} + \hat{T}_{mf,h2} \Re\{F_3 + F_4\} \right)$$
 (32)

where F_1 and F_2 are the terms due to harmonic h_1 , and F_3 and F_4 are the terms due to harmonic h_2 :

$$F_1 = \sum_{k=1}^{m} e^{j(2\theta - [p_s + h_1]\alpha_{w,k})}, \ F_2 = \sum_{k=1}^{m} e^{j(p_s - h_1)\alpha_{w,k}}$$
 (33)

$$F_3 = \sum_{k=1}^{m} e^{j(2\theta - [p_s + h_2]\alpha_{\mathbf{w},k})}, \ F_4 = \sum_{k=1}^{m} e^{j(p_s - h_2)\alpha_{\mathbf{w},k}}$$
(34)

If Table I's symmetry requirements are satisfied, $F_1 = F_3 = 0$ and therefore force is constant over all rotor angles:

$$F_x = k_f I_x, \ k_f = \frac{m\hat{T}_{mf}}{2}$$
 (35)

where k_f is a force per ampere constant. For windings that violate $\frac{2p}{m} \notin \mathbb{N}$ of (26), the net force expression becomes:

$$F_x = k_f I_x + k_{f,h} I_x \cos(2[\theta - p\alpha_{w0}])$$
 (36)

which shows that these windings have an additional force ripple component as there is a dependence on the rotor angle θ (non-zero F_1 or F_3). This is due to the suspension currents creating magnetic fields at both harmonics h_1 and h_2 , which rotate in opposite directions. One harmonic interacts with the rotor p pole-pair field to create non-zero average force, while another harmonic causes the force ripple.

This provides a theoretical explanation for the force ripple reported in [24] for a m=3 machine. Too large of force ripple (or force vector error) can lead to suspension instability. However, by solving (36), advanced control techniques can be implemented to reduce the force ripple, analogous to what is proposed in [24, Sec III-B]. Apart from controls, machine design techniques may also be used to reduce force ripple by minimizing $k_{f,h}/k_f$ in (36). From (15) and (35), it can be shown that setting $p_s=h_2$ and constraining the machine parameters to $h_1\delta=r$ will eliminate force ripple due to h_1 . This simplifies (36) to have the same expression as (35).

In summary, while it is possible to create designs with m=3 or 4 drive connections, these machines will nearly always have higher torque and force ripple as compared to $m \ge 5$.

TABLE I MP COMBINED WINDING DESIGN REQUIREMENTS

Requirement	Standard	New ^a
Symmetry	$z_c/m \in \mathbb{N}$	$\begin{array}{c} 2p/m \notin \mathbb{N} \\ 2p_s/m \notin \mathbb{N} \end{array}$
Independent force/torque creation		$(p+p_s)/m \notin \mathbb{N}$

^aWhile only m > 5 phases satisfy these requirements, Section V-A3 shows that m = 3, 4 is possible when "single-phase" characteristics are acceptable.

B. Independent force/torque creation requirements

Further restrictions are placed on the machine to ensure that the MP winding can independently control force and torque. This requires $T_{md}i_t = 0$ and $T_{mt}i_s = 0$. Using expressions developed for T_m matrix entries and the phase currents, the above constraint equations can be rewritten analogous to the equations (28) and (32) and used to determine conditions for independent force/torque creation. After doing these substitutions, it can be shown that the above constraints are satisfied if the following two constraints are met:

$$\sum_{k=1}^{m} e^{j(\alpha_s - \alpha_t)[k-1]} = 0$$

$$\sum_{k=1}^{m} e^{j(2\theta - [\alpha_s + \alpha_t][k-1])} = 0$$
(37)

$$\sum_{k=1}^{m} e^{j(2\theta - [\alpha_s + \alpha_t][k-1])} = 0$$
 (38)

Condition (37) is always satisfied since from (20) $\alpha_s - \alpha_t =$ $\pm 2\pi/m$. Condition (38) is violated only if $\alpha_s + \alpha_t$ is a multiple of 2π . In this case, (38) is equal to $me^{j2\theta}$, resulting in a pulsating torque (at 2θ) due to force creating currents and a pulsating force due to torque currents. Otherwise, if $\alpha_s + \alpha_t$ is not a multiple of 2π , (38) is always satisfied because the terms in the sum form a balanced set of vectors in the complex plane with a phase separation of $\frac{2\pi}{m}(p+p_s)$. The following constraint is proposed to ensure independent force/torque creation:

$$\frac{p+p_s}{m} \notin \mathbb{N} \tag{39}$$

This requirement is listed in Table I (row 4 column 3).

VI. COMPARISON TO DPNV WINDING

The MP and DPNV windings are viewed as providing the highest performance potential combined winding because of their ability to independently control field weakening as well as torque and force. Recently, reference [22, Sec III-C) has made the observation that DPNV drives/windings [14] can be viewed as a circuit-based connection of certain MP combined windings. It was noted that the DPNV drive resulted in equivalent coil currents (and therefore, equivalent airgap fields, force, and torque). This implies that the DPNV winding design [14] must actually be equivalent to these MP combined windings. This notion is now explored by showing the equivalence (and differences) in winding design requirements between Table I and [14, Tables II-IV]. Based on this comparison, this section will identify design criteria that allow an MP combined winding to be operated from a DPNV drive, which is the second key contribution of this paper.

Upon inspecting the DPNV winding, it is immediately evident that it requires an even number of connections to the motor drive electronics, and therefore winding equivalence is

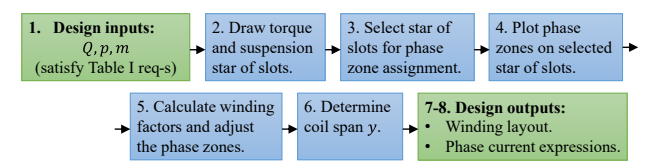


Fig. 4. Summary of MP combined winding design steps.

only possible for an even value of m. Each of the three DPNV requirement tables is now considered. In this description, mretains the definition used in this paper (the total number of drive connections), which is different from the definition of m in [14]. Further, although it is not immediately obvious, it can be shown that the DPNV winding design always results in $\alpha_{\rm ph,w} = \frac{2\pi}{m/2}$, in juxtaposition to (20).

- 1) Symmetry: The DPNV winding requires that $p \perp m/2$ and $p_s \perp m/2$ (\perp means co-prime) [14, Table II]. While this requirement satisfies the symmetry requirements of MP combined windings (Table I), it is more restrictive. The DPNV winding needs this more restrictive requirement to ensure that the winding always has an effective number of torque and suspension phases such that $m_t = m_s = m/2$ to support the DPNV drive connection style-see [14, Fig. 1]. The proof of this can be arrived at by noting that since $\alpha_{\rm ph,w}=\frac{2\pi}{m/2}$, the torque and suspension phases in the DPNV winding are phase separated by $\alpha_t=p\frac{2\pi}{m/2}$ and $\alpha_s=p_s\frac{2\pi}{m/2}$. Similar to the discussion in Section IV-C2, the effective number of phases in the DPNV winding are found by reducing $\frac{p}{m/2}$ or $\frac{p_s}{m/2}$ until the numerator and denominator are co-prime.
- 2) No-Voltage: [14, Table III] summarizes these requirements and it can be shown that these requirements are equivalent to MP winding requirements when m is even.
- 3) Non-zero suspension distribution factor: [14, Table IV] summarizes these requirements. Again, it can be shown that these are equivalent to MP combined windings when m is even. This means that MP combined windings also have the property that there will always be phasors 360° apart in the torque star that are 180° apart in the suspension star (or vice versa), matching [14, Table IV] for $p_s = p \pm 1$ machines.

In summary, the DPNV winding can be viewed as a special case of the MP combined winding. Any MP combined winding that has $p \perp m/2$ and $p_s \perp m/2$ in addition to the requirements in Table I is equivalent to a DPNV winding and can therefore be operated using the DPNV drive configurations of [14, Fig. 1].

VII. PROPOSED WINDING DESIGN APPROACH

This section proposes a design procedure to enable a bearingless motor designer to determine a feasible winding layout for any desired MP combined winding. This is a third and main contribution of this paper. A set of design steps is first provided followed by examples that utilize these steps.

A. Design Steps

The proposed winding design approach is intended for double-layer windings, where each slot holds two coil sides. The new design approach is inspired by the popular "star of slots" design used in convenional windings [15, Chapter 2.2]

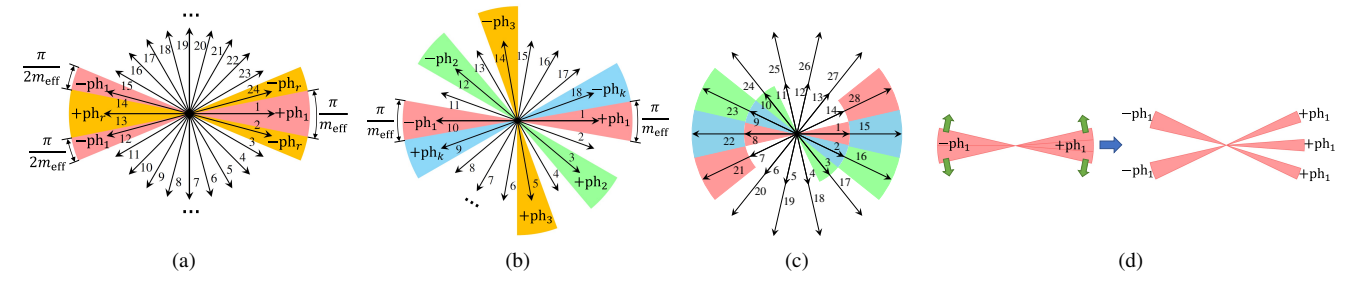


Fig. 5. Illustration of design steps 4 and 5. Step 4: phase zones for case (a), (b), and (c). Step 5: (d) modifications to positive and negative phase zones. and makes use of the torque and suspension star of slots diagrams developed in Section IV-B. The proposed design steps are as followings (summarized in Fig. 4):

- 1) Select motor parameters that satisfy Table I requirements: Slots Q, pole-pairs (p and p_s), and phases m.
- 2) Draw torque / suspension star of slots diagrams: Refer to the procedure in the discussion accompanying Fig. 3.
- 3) Select star of slots for phase zone assignment: Identify the star with the highest number of phasors in a layer per effective number of phases: $\max\left(\frac{Q}{\gcd(Q,p)m_t},\frac{Q}{\gcd(Q,p_s)m_s}\right)$, with m_t, m_s from (21). Define $m_{\rm eff}$ as the effective number of phases of the selected star $(m_t \text{ or } m_s)$.
- 4) Plot phase zones on selected star of slots: Assign each phasor (coil-side) in the star of slots identified in step 4 to a phase by drawing positive and negative phase zones on top of the star. Draw the phase zones following one of these cases:
 - a) Designs with even m_{eff} : Plot the phase zone diagram as in Fig. 5a. Since there are always pairs of phases separated by π radians for even $m_{\rm eff}$, the negative phase zone for each phase has to be split into two parts as shown in Fig. 5a.
 - b) Designs with odd $m_{\rm eff}$ and with at least one of the following conditions satisfied: $m_t \neq m_s$, gcd(Q, p) = 1, or $gcd(Q, p_s) = 1$. Plot the phase zone diagram as in Fig. 5b. The positive and negative phase zones span $\pi/m_{\rm eff}$ and are separated by π radians. The adjacent positive (negative) phase zones are separated by $2\pi/m_{\rm eff}$.
 - c) All other designs with odd m_{eff} : Draw the star of slots in several layers (in the radial direction) and plot the phase zones in each layer separately, as shown in Fig. 5c. Note that each layer uses the same phase zone assignment as in Fig. 5b, but has a different angular orientation.
- 5) Calculate winding factors and adjust the phase zones: Use (18) to calculate the torque k_{dt} , suspension k_{ds} distribution factors. If these are unacceptably low, try the following:

First, slightly rotate the phase zones in Fig. 5a-5b clockwise or counterclockwise and select the phase-zone assignment that gives the highest distribution factors.

Next, if the distribution factors remain unacceptable, split positive and/or negative phase zones into several parts and rotate away from each other so that the net positive and negative phase zone orientations are unchanged—see Fig. 5d. Rotate these bands in increments that correspond to their bandwidth. This ensures equal phase band area for all phases and proper phase separation. Stop when satisfactory distribution factors are obtained. The other phases' zones can be found by rotating the phase 1 by $(k-1)2\pi/m_{\text{eff}}$ $(k=2 \text{ to } m_{\text{eff}})$.

6) Determine coil span: Identify a coil span y (number of slots) that achieves the preferred compromise between torque \vec{k}_{pt} and suspension \vec{k}_{ps} pitch factors. Calculate \vec{k}_{pt} and \vec{k}_{ps} for different y values by setting h = p, p_s in (18). Ensure that $yp/Q \notin \mathbb{N}$ and $yp_s/Q \notin \mathbb{N}$ to avoid zero pitch factors.

After following steps 1-6, it is possible to have multiple candidate designs for a specific slot-pole combination. To choose one design, the designer is advised to consider winding factors $k_{w,p}$ and k_{w,p_s} for torque p and suspension p_s pole pairs. Ideally, a designer would choose an option with both highest $k_{w,p}$ and k_{w,p_s} (if such a design exists) to obtain the maximum torque- and force-per-ampere. In other cases when there is a trade-off between $k_{w,p}$ and k_{w,p_s} across different designs, the choice depends on the motor's required torque and force ratings. For most applications, it is suggested to select a design with a relatively higher $k_{w,p}$ (> 0.7) and a reasonable k_{w,p_s} value (> 0.4 – 0.5).

- 7) Construct winding layout diagram: Determine the coil connections for each phase using the results from steps 4-6. Each phase coil has two coil sides. The slot location of one coil side is determined by the phase zone diagram, while the slot location of the other coil side is determined by the coil span y. The coils in each phase are connected in series.
- 8) Determine the phase current expressions: The phase currents consist of torque and suspension force creating components. The torque and suspension phase angles $\alpha_t = p \frac{2\pi}{m}$ and $\alpha_s = p_s \frac{2\pi}{m}$ in (20) determine which phase currents to flow through the coils to create two rotating magnetic field pole-pairs. The phase current k has the following expression:

$$i_k = I_t \cos(\phi_t - [k-1]\alpha_t) + I_s \cos(\phi_s - [k-1]\alpha_s)$$
 (40)

B. Example designs

The proposed design steps are now demonstrated for a double-layer winding with Q = 12, p = 2, $p_s = 1$, and m = 6:

- 1) From (23), $z_c = 12$; Table I design requirements are met.
- 2) The diagrams are shown in Fig. 6a and 6c. The mechanical angle between adjacent slots is $\alpha_u = \pi/6$, resulting in $\pi/3$ in the torque and $\pi/6$ in the suspension star of slots.
- 3) Both torque and suspension stars have two phasors in a layer per effective number of phases $(m_t = 3, m_s = 6)$. Therefore, either of the stars can be selected. For this example, the torque star of slots is selected and $m_{\text{eff}} = 3$.
- 4) This example uses case b) described Section VII-A4 for drawing the phase zones. Since $m_{\rm eff}=3$, each phase zone spans $\pi/m_{\rm eff} = \pi/3$ radians. The positive and negative phase zones are plotted in Fig. 6a, where the phases are labeled from u to z. Note that each phase zone has two identical phases in

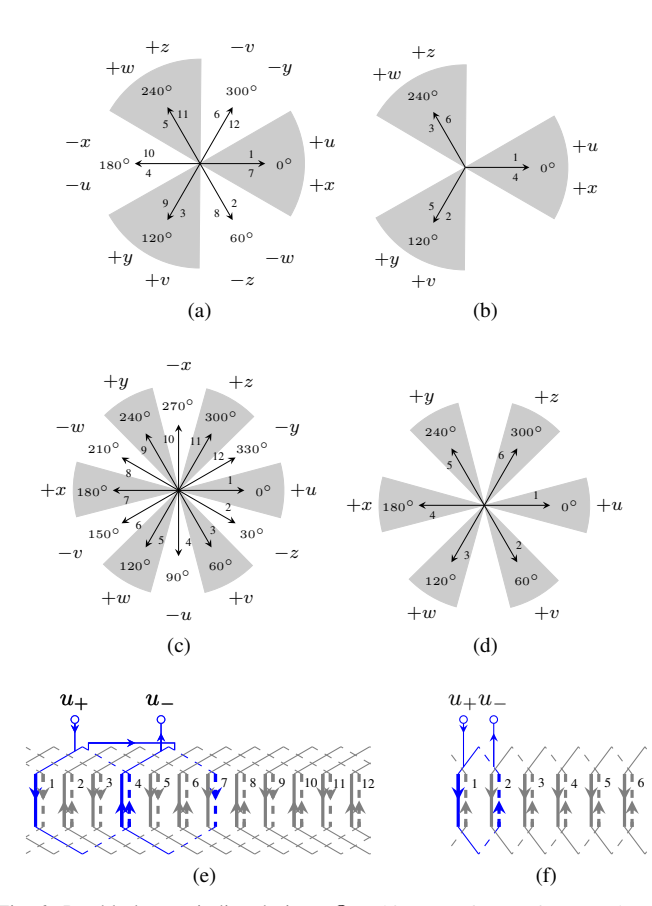


Fig. 6. Double-layer winding designs. $Q=12,\ m=6,\ p=2,\ p_s=1,$ and y=3: (a) torque star of slots; (c) suspension star of slots; and (e) winding layout. $Q=6,\ m=6,\ p=2,\ p_s=1,$ and y=1: (b) torque star of slots; (d) suspension star of slots; and (f) winding layout.

the torque star. Therefore, half of the slots in each zone are assigned to each phase. The resulting star diagrams are shown in Fig. 6a and 6c.

- 5) The torque, suspension distribution factors are calculated as $\hat{k}_{dt}=1$, $\hat{k}_{ds}=0.707$. It is determined that these are satisfactory and no phase zone modification is needed.
- 6) The coil span is selected as y=3, yielding $\hat{k}_{pt}=\sin\left(\frac{y\pi}{6}\right)=1$ and $\hat{k}_{ps}=\sin\left(\frac{y\pi}{12}\right)=0.707$. The resulting torque, suspension winding factors are $\hat{k}_{wt}=1$, $\hat{k}_{ws}=0.5$.
 - 7) The resulting phase u winding layout is shown in Fig. 6e.
- 8) The phase current expressions are determined by (40) with $\alpha_t=\frac{2\pi}{3}$ and $\alpha_s=\frac{\pi}{3}$.

The design procedure can similarly be used to design any MP combined windings satisfying the Table I requirements. A second example design with concentrated windings is given in Fig. 6f (with star of slots in Fig. 6b and 6d). A third and fourth example are shown in Fig. 7 (m=7, 8), where this time the suspension star of slots is selected in step 3 for phase zone assignment in step 4. These last two examples depict adjusting the phase zones in step 5 to increase the torque distribution factor. In a fifth example, Fig. 8 presents a distributed winding with m=6, Q=24, where only positive phase zones are used. This winding design is used in the bearingless induction machine prototype presented in Section VIII.

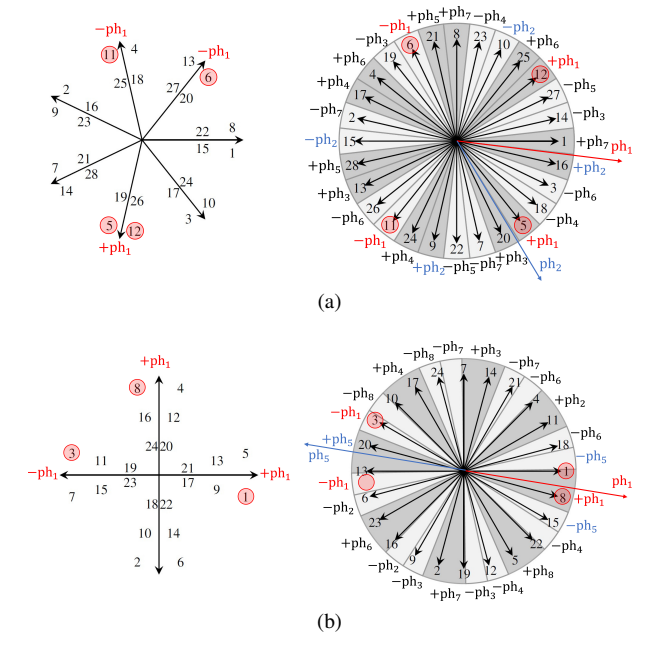


Fig. 7. Torque (left) and suspension (right) star of slots for two examples that illustrate design steps 4 and 5 (dark gray – positive phase zones, light gray – negative phase zones): (a) $Q=28,\ m=7,\ p=16,$ and $p_s=15$ ($m_t=m_s=7$) and (b) $Q=24,\ m=8,\ p=6,$ and $p_s=7$ ($m_t=4,\ m_s=8$). The red circles show the slots assigned to phase 1.

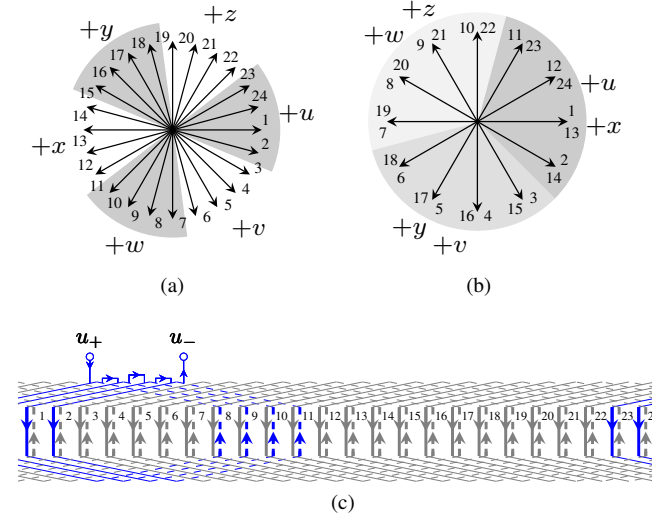


Fig. 8. Design of Q=24, m=6, p=1, $p_s=2$, y=9 double-layer winding of the induction machine prototype used for validation in Section VIII: (a) torque; (b) suspension star of slots; and (c) winding layout.

VIII. VALIDATION OF MP COMBINED WINDING DESIGN

Validation is now provided using finite element analysis and experimental measurements of a pole-specific bearingless induction motor prototype, shown in Fig. 11a. This machine's winding is implemented as the six-phase combined winding presented in Fig. 8c. The phase currents required to create p=1 and $p_s=2$ pole-pair fields in the airgap of this machine are given by the following equation—see (40):

$$i_k = I_t \cos\left(\phi_t - [k-1]\frac{2\pi}{6}\right) + I_s \cos\left(\phi_s - [k-1]\frac{2\pi}{3}\right)$$
 (41)

where
$$k = 1$$
 to 6, $I_t = \sqrt{i_d^2 + i_q^2}$.

This winding satisfies the criteria to be operated by a DPNV drive that were derived in Section VI. Additional machine

TABLE II
INDUCTION MOTOR PROTOTYPE PARAMETERS

Rated i_d	6.75 A	Rated i_q	5.85 A
Force per current k_f^a	13 N/A	Torque per current k_t	0.2 Nm/A
Rated slip frequency	12.5 Hz	Rated speed	29250 RPM

 ak_f and k_t are measured at the rated i_d value.

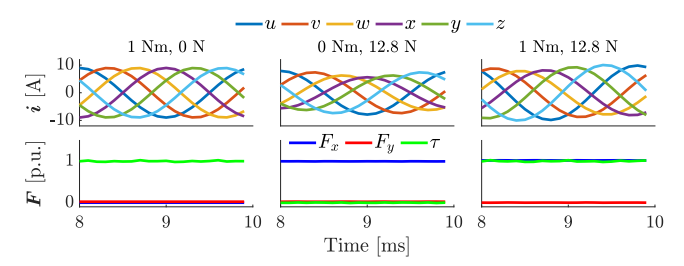


Fig. 9. FEA results for example six-phase induction machine prototype: calculated torque and force for different currents (column 1-rated torque, column 2-rated force, column 3-rated torque and force). $F_{\rm base}=12.8~{\rm N},$ $\tau_{\rm base}=1~{\rm Nm}.$

design information is provided in [23], [26], which presented test results obtained with the machine operated by a three-phase parallel DPNV drive. The key motor parameters are summarized in Table II when the winding is configured for operation by a six-phase drive. In the following tests, the machine is excited with various phase currents to create desired airgap fields and torque and force vectors, with measurements compared against the findings of Sections III-VII to confirm the theoretic developments of this paper.

A. FEA Simulations

The proper operation of the example MP combined winding (if symmetry and independent force/torque creation are met) is now demonstrated using FEA simulation results for three different cases of phase currents, all described by (41). In all cases, currents have $\phi_t = \phi_s = 2\pi ft$ with a rated frequency of f=500 Hz and a rated magnetizing current $i_d=6.75$ A. The first column of Fig. 9 shows that only torque is produced when the rated torque creating current $i_q=5.85$ A is applied (rated rotor speed and slip). The second column shows that only force is produced when the rated suspension current $I_s=1.15$ A is applied (zero slip). The third column shows that both torque and force are produced when rated i_q and I_s are present (rated slip).

B. Experimental Validation

Three test results are presented that confirm that the airgap magnetic fields with the desired pole-pairs $(p=1, p_s=2)$ can be created, that force and torque can be created independently, and that MP and DPNV combined windings are equivalent. These tests validate the theory developed in Sections V-VII. In all tests, the phase windings are excited by the currents described by (41).

1) Magnetic field measurements: This test is conducted to validate the MP combined winding symmetry requirement that two rotating p and p_s pole-pair fields are created when the phase currents are supplied by a symmetrical supply, as defined in Section II and summarized in Table I. In this test, the normal

airgap magnetic field $B_{\rm n}$ is measured with a hall probe [27] in front of each tooth (15° increment) along the inner bore of the stator (along α), as shown in Fig. 10a. Despite the rotor not being present in Fig. 10a, it is fully inserted during the test. At each tooth, measurements are taken for the following two cases of excitation–see (41):

- 1) $I_t=13.5$ A, $I_s=0$ with ϕ_t swept over $0-2\pi$ rad. (expected to create p=1 pole-pair field).
- 2) $I_s = 13.5$ A, $I_t = 0$ with ϕ_s swept over $0 2\pi$ rad. (expected to create $p_s = 2$ pole-pair field).

The result for case 1 is provided in Fig. 10b, which shows a 3D plot of the measured normal magnetic field $B_{\rm n}$ as a function of α and ϕ_t . This plot shows that the airgap field has p=1 pole-pair when viewed along α at any fixed ϕ_t value. As an example, Fig. 10d plots a special case of Fig. 10b for $\phi_t=60^\circ$ (in blue) to show that p=1 pole-pair is created. As ϕ_t increases, the angular location of the field along α in Fig. 10b also increases according to $\alpha_{\rm peak}=\phi_t/p$ and the field behavior can be described by the rotating field equation $B_{\rm n}=0.65\cos(\alpha-\phi_t)$ [T].

Figure 10c provides a similar 3D plot of B_n for case 2 as a function of α and ϕ_s . This plot shows that the airgap field has $p_s=2$ pole-pairs when viewed along α at any fixed ϕ_s value. Figure 10d again plots the special case of Fig. 10c for $\phi_s=60^\circ$ (in red) to show that $p_s=2$ pole-pair is created. Analogous to case 1, the angular location of the field along α in 10c increases by increasing ϕ_s according to $\alpha_{\rm peak}=\phi_s/p_s$ and the field behavior is described by the rotating field equation $B_n=0.2\cos(2\alpha-\phi_s)$ [T].

The observations made above validate the MP combined winding symmetry requirements (see Table I) that rotating p and p_s pole-pair fields can be created when motor windings are excited by balanced currents.

- 2) Force and torque measurements: The results of this test validate the MP combined winding independent force and torque creation requirements, as defined in Section II and summarized in Table I. In this test, reaction torque and forces on the stator are measured using a load cell [28], as shown in Fig. 11a. The stator is mounted on the load cell, which is rigidly fixed. The rotor is supported by a mill's spindle and locked at the magnetic center in a manner that prevents rotation and deflection. The injected phase currents are described by (41) with $\phi_t = 2\pi ft$ and $\phi_s = 2\pi ft + \phi$. The measurements are taken for the following two cases:
 - 1) f = 0.10 Hz, $I_t = 6.75$ A, $I_s = 1.15$ A (see Fig. 11b, column 1). This test verifies that rated force can be created at any angle. The frequency is set to a sufficiently low value so that no torque is created.
 - 2) f=12.5, $I_t=9.10$ A, $I_s=1.15$ A (see Fig. 11b, column 2). This test verifies that rated force can be created at any angle while torque is also produced. Since the rotor is locked, the motor operates under rated slip frequency (see Table II).

In both cases, the motor is expected to have $i_d=6.75$ A. During the tests, ϕ is set to a fixed value, forces and torque are measured at steady state, and the average is calculated.

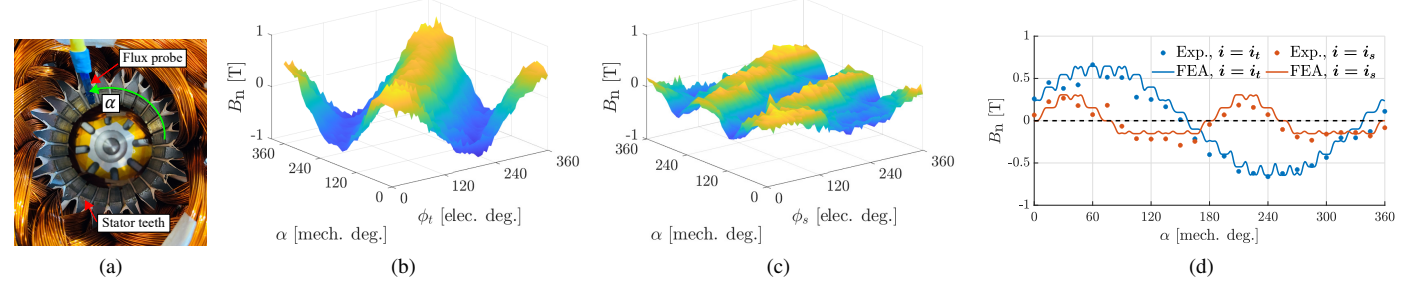


Fig. 10. Experimentally measured magnetic field: (a) test setup; B_n when (b) torque currents are present ($i = i_t$); (c) suspension currents are present ($i = i_s$), and (d) torque and suspension currents are present with $\phi_t = 60^\circ$ and $\phi_s = 60^\circ$ (obtained from Fig. 10b-10c).

The measurements are repeated for the values of ϕ from 0 to 2π rad. with an increment of $\pi/6$ rad.

Figure 11c provides measurement results of the forces F_x , F_y , and torque τ vs. ϕ for the two cases described above. Figure 11d is a plot of the force vector magnitude and angle obtained using the Fig. 11c results. These results show that the force vector angle can be changed by modifying ϕ while having no effect on torque. The reverse is also true—whether torque is being created or not, the motor can independently create force vectors with a constant magnitude at any angle. It has also been confirmed that the motor creates zero average force when $I_s=0$ A. Together, these results indicate that force and torque creation can be created independently by controlling (I_s, ϕ) and i_q (with a constant i_d), which validate the independent force and torque creation requirements summarized in (39) and Table I.

3) Comparison to DPNV Winding: This test validates equivalence between MP and DPNV combined windings (see Section VI) using suspension force measurements. As summarized in Section VI, an MP combined winding must additionally satisfy $p \perp m/2$ and $p_s \perp m/2$ to be capable of operation by a DPNV drive. The winding of this prototype (see Fig. 8c) meets these additional design criteria because $p=1, p_s=2$, and m=6 (1 \perp 3 and 2 \perp 3). The sixphase MP currents $[i_1, i_2, i_3, i_4, i_5, i_6]^T$ in (41) map to the DPNV coil group currents in [14] in the following order as $[i_{u_b}, -i_{w_a}, i_{v_b}, -i_{u_a}, i_{w_b}, -i_{v_a}]^T$ —see Fig. 12.

The required DPNV drive torque $i_{t,k}$ and suspension $i_{s,k}$ terminal currents (see Fig. 12) are expressed as:

$$i_{t,k} = 2I_t \cos\left(\phi_t - [k-1]\frac{2\pi}{3}\right)$$

$$i_{s,k} = I_s \cos\left(\phi_s + [k-1]\frac{2\pi}{3}\right) - I_t \cos\left(\phi_t - [k-1]\frac{2\pi}{3}\right)$$
(42)

where k=1 to 3. This drive connection configuration is compelling because it allows the inverter responsible for providing i_t to be implemented as a standard three phase motor drive without knowledge of the machine being bearingless. This is because the i_t terminals contain only a single sequence current $(2\pi/3 \text{ spacing})$ as compared to the current expressions in (41) which have two sequences. Note that when the DPNV drive provides currents according to (42), the machine coils will have the same currents as when the MP drive provides currents according to (41), meaning that the machine has identical torque and force performance.

Test results are now presented to validate that the machine is capable of actuating force and torque identically, regardless of whether it is connected as an MP or parallel DPNV drive. First, the measured suspension force produced by the machine using both styles of drive is plotted in Fig. 11e, with drive phase currents determined by (41) and (42). Rated i_d current is applied, $i_q = 0$ A, over a range of I_s values. The slope of this curve determines the force created per unit current $k_f = 13$ N/A, listed in Table II. The red marker in Fig. 11e represents the force measured when the prototype is operated by the six-phase MP drive (tested at rated suspension current $I_s = 1.15 \text{ A}$) while the blue dots correspond to measurements when the prototype is operated by the parallel DPNV drive (see Fig. 12). Clearly both drives result in the machine having the same force characteristic. A similar test was conducted to compare the torque capability of the machine, resulting in identical torque per unit current $k_t = 0.2 \text{Nm/A}$, listed in Table II. By demonstrating that both drives are able to identically actuate force and torque, these results validate the design criteria derived in Section VI for when an MP combined winding can be operated by a DPNV drive.

IX. CONCLUSION

Historically, challenges in the winding design for bearingless motors have limited the machine performance (torque density, torque and force ripple, and efficiency). Combined windings are gaining attention as a potential solution for these problems, with MP combined windings being widely recognized as one of the highest performance approaches. This paper develops the fundamental force/torque model for machines employing these windings and uses this model to establish a winding analysis framework, machine design requirements, and winding design theory, which are the main contributions of this paper.

While it is found that many combinations of stator slots, poles, and phases can lead to viable windings, certain combinations lead to either asymmetric windings or cross-coupling between the motor and suspension operation. The highest performance MP winding designs have at least five connections to the drive electronics. However, this paper's analysis framework shows that it is possible to reduce this to three or four connections (presumably to save cost) and obtain an asymmetric winding that is feasible, but with higher torque and force ripple. It is found that the classical star of slots design methodology for stator windings can be extended to aid in

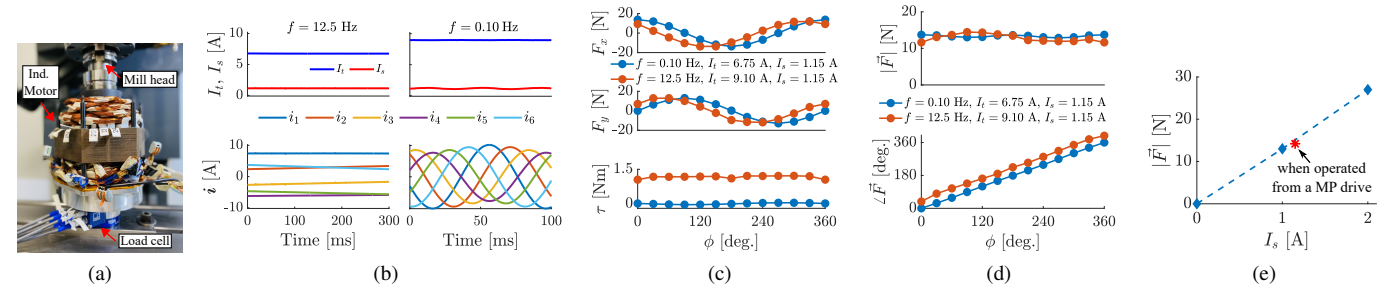


Fig. 11. Experiment results of the force and torque measurements: (a) test setup, (b) phase currents for two cases of test 2, (c)-(d) measured forces and torque for different ϕ values, and (e) measured force vs. suspension current for MP drive (red) and DPNV drive (blue).

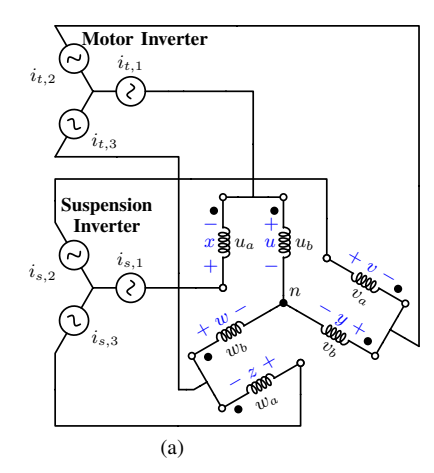


Fig. 12. The prototype machine's winding configured for operation by a parallel DPNV drive. The 6 phases from Fig. 8c u, v, w, x, y, z are shown in blue to indicate their mapping to the DPNV coil groups a and b [22].

the design of MP combined windings by considering both the motor and suspension field spatial harmonics. Experimental results from a six-phase induction machine validate the MP combined winding analysis framework and design approach.

Motor designers will find this paper useful as a practical guide to rapidly design MP combined windings for various slot-pole combination motors. Its general analysis framework and repeatable design steps enable consideration of a large number of machine variants.

REFERENCES

- A. Chiba, T. Fukao, O. Ichikawa, M. Oshima, M. Takemoto, and D. Dorrell, Magnetic Bearings and Bearingless Drives. Newnes, 2005.
- [2] S. Silber, W. Amrhein, P. Bosch, R. Schob, and N. Barletta, "Design aspects of bearingless slice motors," *IEEE/ASME Transactions on Mechatronics*, vol. 10, no. 6, pp. 611–617, Dec 2005.
- [3] D. Dietz and A. Binder, "Comparison between a bearingless pm motor with separated and combined winding for torque and lateral force generation," in 2019 21st European Conference on Power Electronics and Applications (EPE'19 ECCE Europe). IEEE, 2019, pp. P-1.
- [4] W. Gruber, T. Nussbaumer, H. Grabner, and W. Amrhein, "Wide air gap and large-scale bearingless segment motor with six stator elements," *IEEE Transactions on Magnetics*, vol. 46, no. 6, pp. 2438–2441, 2010.
- [5] S. Silber and W. Amrhein, "Power optimal current control scheme for bearingless pm motors," in *Proc. 7th Int. Symp. Magn. Bearings*, 2000, pp. 401–406.
- [6] Min Kang, Jin Huang, Hai-bo Jiang, and Jia-qiang Yang, "Principle and simulation of a 5-phase bearingless permanent magnet-type synchronous motor," in 2008 International Conference on Electrical Machines and Systems, 2008, pp. 1148–1152.

- [7] V. F. Victor, J. de Paiva, A. O. Salazar, and A. L. Maitelli, "Performance analysis of a neural flux observer for a bearingless induction machine with divided windings," in 2009 Brazilian Power Electronics Conference, 2009, pp. 498–504.
- [8] W. K. S. Khoo, "Bridge configured winding for polyphase self-bearing machines," *IEEE Transactions on Magnetics*, vol. 41, no. 4, pp. 1289– 1295, 2005.
- [9] R. Oishi, S. Horima, H. Sugimoto, and A. Chiba, "A novel parallel motor winding structure for bearingless motors," *Magnetics, IEEE Transactions* on, vol. 49, no. 5, pp. 2287–2290, 2013.
- [10] E. Severson, S. Gandikota, and N. Mohan, "Practical implementation of dual-purpose no-voltage drives for bearingless motors," *IEEE Transactions on Industry Applications*, vol. 52, no. 2, pp. 1509–1518, March 2016.
- [11] G. Valente, A. Formentini, L. Papini, P. Zanchetta, and C. Gerada, "Position control study of a bearingless multi-sector permanent magnet machine," in *IECON* 2017 - 43rd Annual Conference of the *IEEE* Industrial Electronics Society, 2017, pp. 8808–8813.
- [12] A. Chiba, K. Sotome, Y. Iiyama, and M. Azizur Rahman, "A novel middle-point-current-injection-type bearingless pm synchronous motor for vibration suppression," *Industry Applications, IEEE Transactions on*, vol. 47, no. 4, pp. 1700–1706, 2011.
- [13] W. Gruber and S. Silber, "Dual field-oriented control of bearingless motors with combined winding system," in 2018 International Power Electronics Conference (IPEC-Niigata 2018 -ECCE Asia), May 2018, pp. 4028–4033.
- [14] E. L. Severson, R. Nilssen, T. Undeland, and N. Mohan, "Design of dual purpose no-voltage combined windings for bearingless motors," *IEEE Transactions on Industry Applications*, vol. 53, no. 5, pp. 4368–4379, 2017.
- [15] J. Pyrhonen, T. Jokinen, and V. Hrabovcova, *Design of rotating electrical machines*. John Wiley & Sons, 2013.
- [16] A. Khamitov and E. L. Severson, "Analysis and design of multi-phase combined windings for bearingless machines," in 2021 IEEE Energy Conversion Congress and Exposition (ECCE). IEEE, 2021, pp. 3949– 3956.
- [17] S. Rubino, O. Dordevic, E. Armando, R. Bojoi, and E. Levi, "A novel matrix transformation for decoupled control of modular multiphase pmsm drives," *IEEE Transactions on Power Electronics*, 2020.
- [18] E. Levi, M. Jones, S. N. Vukosavic, and H. A. Toliyat, "A novel concept of a multiphase, multimotor vector controlled drive system supplied from a single voltage source inverter," *IEEE Transactions on Power Electronics*, vol. 19, no. 2, pp. 320–335, 2004.
- [19] E. Levi, R. Bojoi, F. Profumo, H. Toliyat, and S. Williamson, "Multiphase induction motor drives—a technology status review," *IET Electric Power Applications*, vol. 1, no. 4, pp. 489–516, 2007.
- [20] G. Sala, M. Mengoni, G. Rizzoli, L. Zarri, and A. Tani, "Decoupled d-q axes current-sharing control of multi-three-phase induction machines," *IEEE Transactions on Industrial Electronics*, vol. 67, no. 9, pp. 7124– 7134, 2019.
- [21] E. Levi, "Advances in converter control and innovative exploitation of additional degrees of freedom for multiphase machines," *IEEE Transactions on Industrial Electronics*, vol. 63, no. 1, pp. 433–448, 2015.
- [22] A. Khamitov, W. Gruber, G. Bramerdorfer, and E. L. Severson, "Comparison of combined winding strategies for radial non-salient bearingless machines," *IEEE Transactions on Industry Applications*, pp. 1–1, 2021.
- [23] J. Chen, M. W. Johnson, A. Farhan, Z. Wang, Y. Fujii, and E. L.

- Severson, "Reduced axial length pole-specific rotor for bearingless induction machines," *IEEE Transactions on Energy Conversion*, 2022.
- [24] J. Asama, T. Oi, T. Oiwa, and A. Chiba, "Simple driving method for a 2-dof controlled bearingless motor using one three-phase inverter," *IEEE Transactions on Industry Applications*, vol. 54, no. 5, pp. 4365–4376, 2018
- [25] M. T. Bartholet, T. Nussbaumer, S. Silber, and J. W. Kolar, "Comparative evaluation of polyphase bearingless slice motors for fluid-handling applications," *IEEE Transactions on Industry Applications*, vol. 45, no. 5, pp. 1821–1830, 2009.
- [26] J. Chen, Y. Fujii, M. W. Johnson, A. Farhan, and E. L. Severson, "Optimal design of the bearingless induction motor," *IEEE Transactions on Industry Applications*, vol. 57, no. 2, pp. 1375–1388, 2021.
- [27] AN180KIT for AKM HG-106C-2U Hall Element Y axis, Thin, High Magnetic Field Sensor, GMW Associates, 2016. [Online]. Available: https://gmw.com/wp-content/uploads/2019/01/AN180KIT-AKM-HG-106C-2U-92716.pdf
- [28] MCS10, Multicomponent sensor, HBM, 2017. [Online]. Available: http://spectromas.ro/wp-content/uploads/2017/12/Fisatehnica-MCS10.pdf



Anvar Khamitov received the B.Eng. degree in electrical and electronic engineering from the Nazarbayev University, Astana, Kazakhstan, in 2018. He is currently a Ph.D. dissertator in electrical engineering at the University of Wisconsin-Madison, Madison, WI, USA. Anvar is working as a research assistant with Dr. Severson at Wisconsin Electric Machines and Power Electronics Consortium (WEMPEC). His research interests include design, modeling, optimization, and control of electric machines, focusing on bearingless machines and off-

highway vehicle electrification.



Eric L Severson (S'09-M'15) received the B.Sc. and PhD degrees in electrical engineering from the University of Minnesota, Minneapolis, USA in 2008 and 2015, respectively where he also worked as a post doctoral associate through 2016. He is currently an assistant professor at the University of Wisconsin-Madison

Dr. Severson is an associate director of the Wisconsin Electric Machines and Power Electronics Consortium (WEMPEC) and fellow of the Grainger Institute for Engineering. His research interests in-

clude design and control of electric machines and power electronics, with focus areas in magnetic bearings, bearingless motors, flywheel energy storage, and off-highway vehicle electrification.

Dr. Severson is a recipient of the USA National Science Foundation CAREER Award in 2020, the Department of Defense NDSEG fellowship in 2009, and the National Science Foundation Graduate Research Fellowship in 2009.